Supplementary Information for

Designing Type-II p-$SiCC_4$/XO (X = Sn, Pb) van der Waals Heterojunctions with a Built-in Electric Field as Promising Photocatalysts for Highly Efficient Overall Water Splitting

Hongjing Wang,[a] Songsong Sun,[a*] Lei Peng,[b] Yanju Ji,[a] Hao Zhang,[c,d*] Yuanfeng Xu,[a*]

[a] *School of Science, Shandong Jianzhu University, Jinan 250101, Shandong, China.*

[b] *Key Laboratory for Computational Physical Sciences (MOE), Institute of Computational Physical Sciences and Department of Physics, Fudan University, Shanghai 200433, China.*

[c] *College of Future Information Technology and Department of Optical Science and Engineering and Key Laboratory of Micro and Nano Photonic Structures (MOE), Fudan University, Shanghai 200433, China.*

[d] *State Key Laboratory of Photovoltaic Science and Technology, Fudan University, Shanghai 200433, China. and*

Correspondence: sunsongsong21@sdjzu.edu.cn (S. Sun), zhangh@fudan.edu.cn (H. Zhang), xuyuanfeng19@sdjzu.edu.cn (Y.Xu)

Supplementary Figures

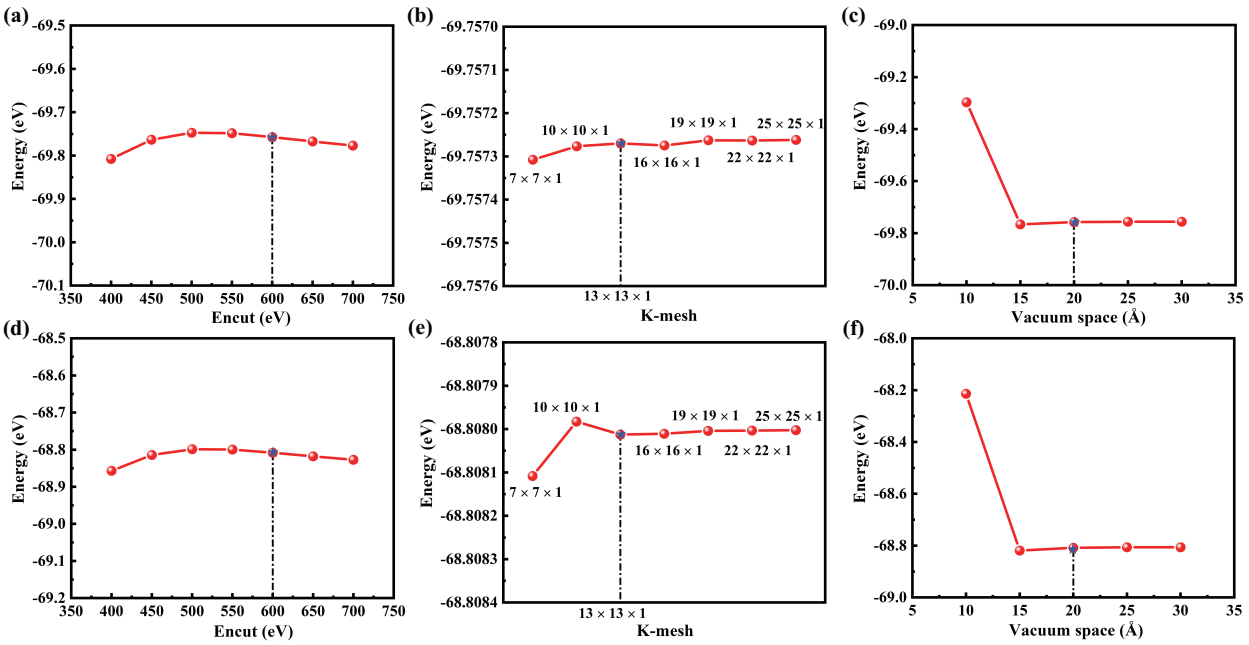

Figure S1. Parameter tests of cutoff energy, k-mesh, and vacuum spacing of for the (a-c) p-$SiCC_4$/SnO and (d-f) p-$SiCC_4$/PbO heterojunctions.

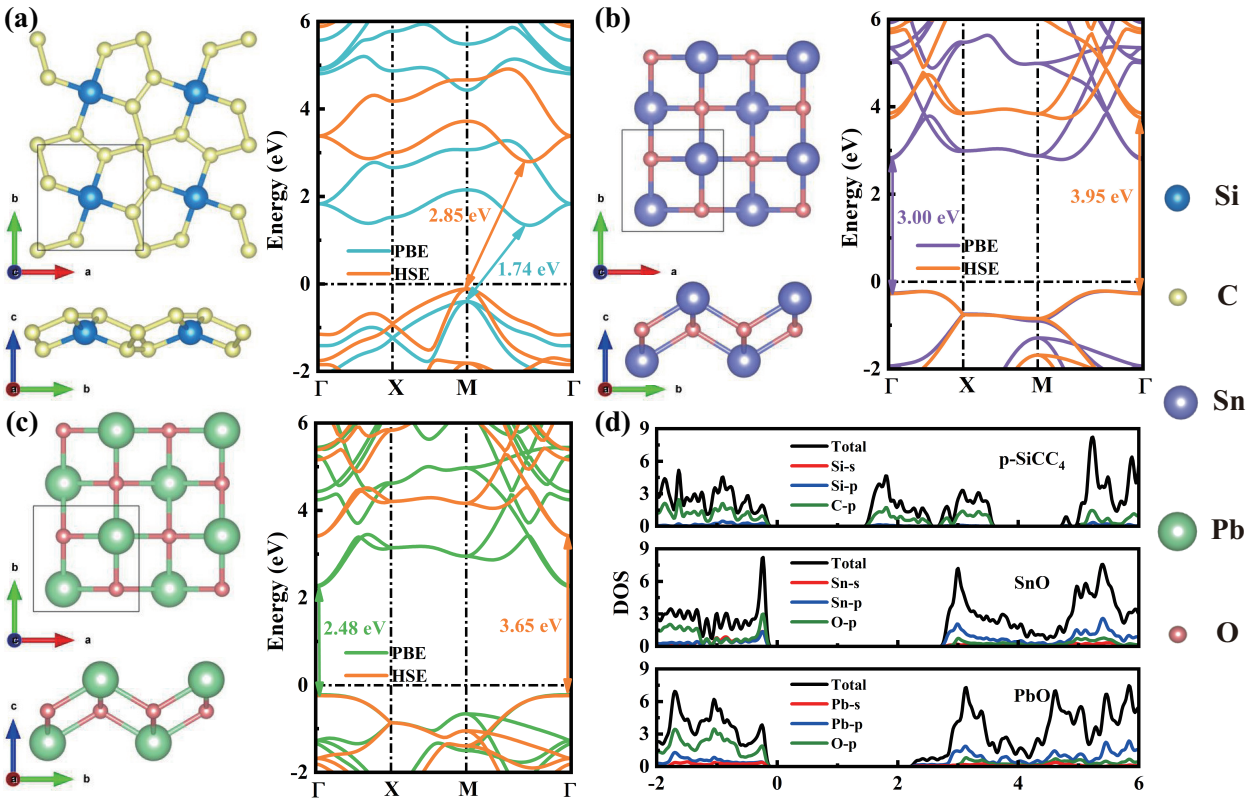

Figure S2. Left panels show the crystal structures of (a) p-$SiCC_4$, (b) SnO, and (c) PbO monolayers, respectively. The middle and right panels depict the band structures of the three monolayers. (d) DOS of the p-$SiCC_4$, SnO, and PbO monolayers.

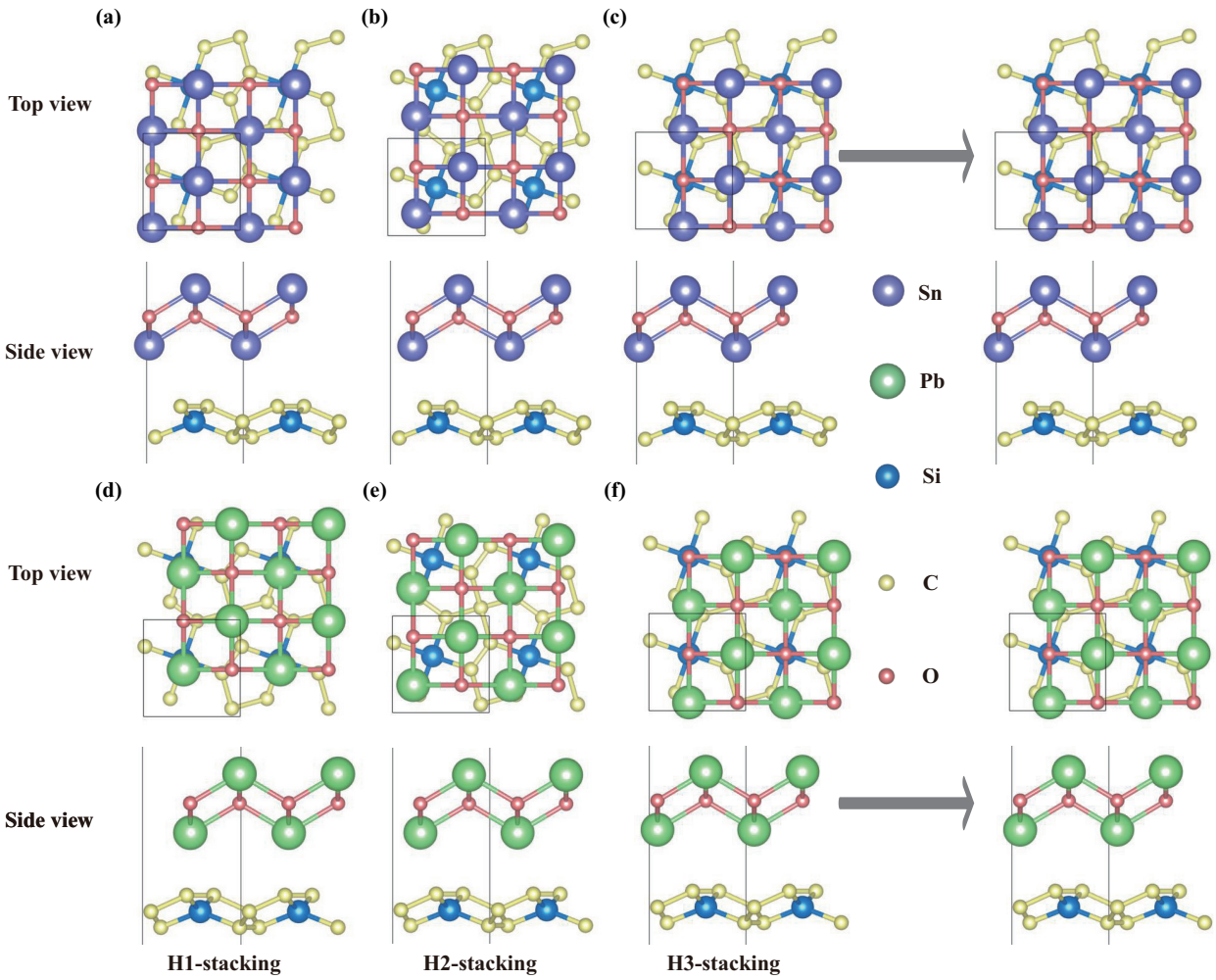

Figure S3. Three high-symmetry stacking configurations, labeled H1, H2, and H3, are considered for the p-$SiCC_4$/XO (X = Sn, Pb) heterojunctions. Following geometric optimization, initial configurations H1 and H2 converged to the H3 stacking geometry. Consequently, the H3 configuration represents the most energetically stable stacking structure identified for these heterojunctions.

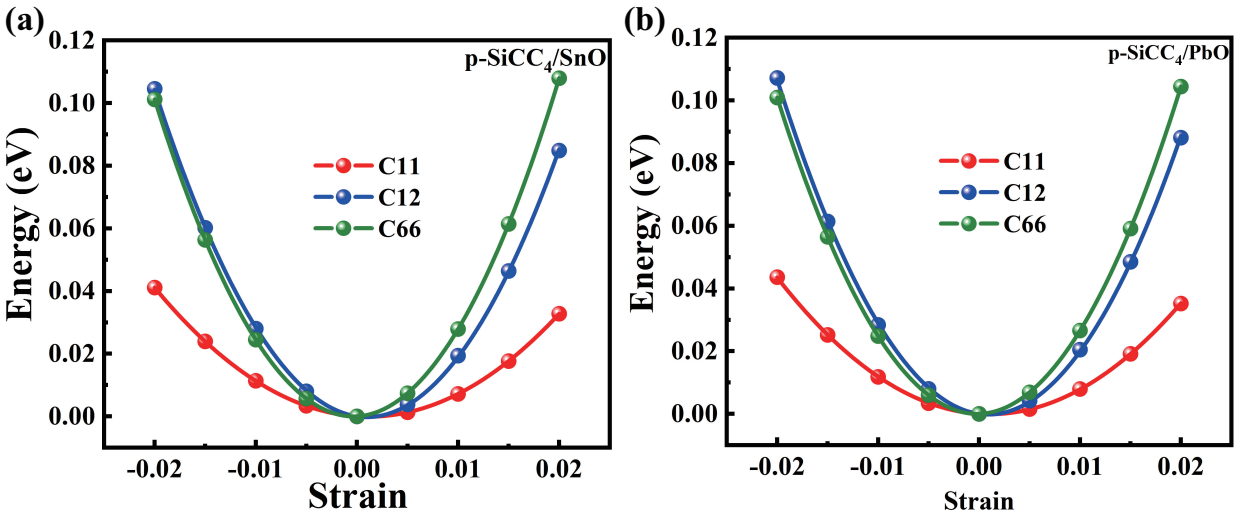

Figure S4. Strain energy of the (a) p-$SiCC_4$/SnO and (b) p-$SiCC_4$/PbO heterojunctions under various strains within the range of -2% $\leq \delta \leq$ 2%. The uniaxial strain curves are calculated by fixing the transverse lattice constant.

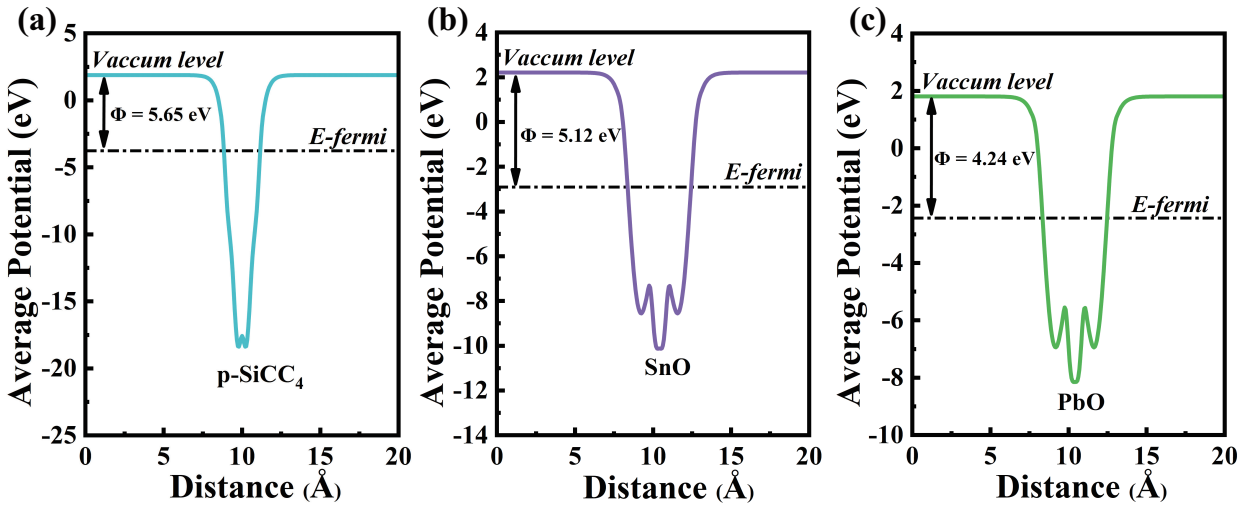

Figure S5. The electrostatic potential diagrams of p-$SiCC_4$, SnO, and PbO monolayers.

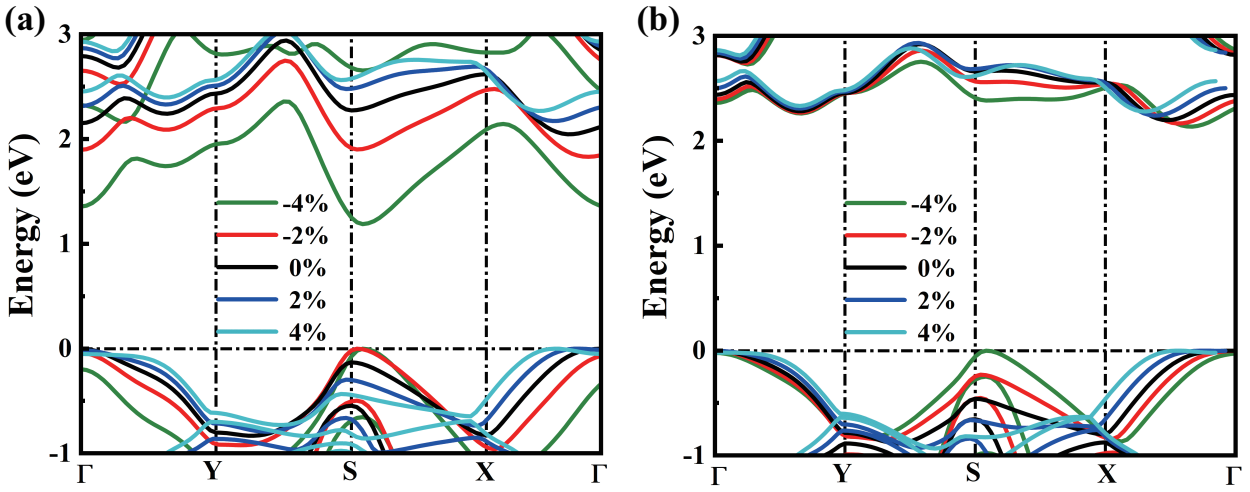

Figure S6. Strain-dependent evolution of energy band diagrams for (a) p-$SiCC_4$/SnO and (b) p-$SiCC_4$/PbO heterojunctions under biaxial strain, as calculated at the HSE06 level.

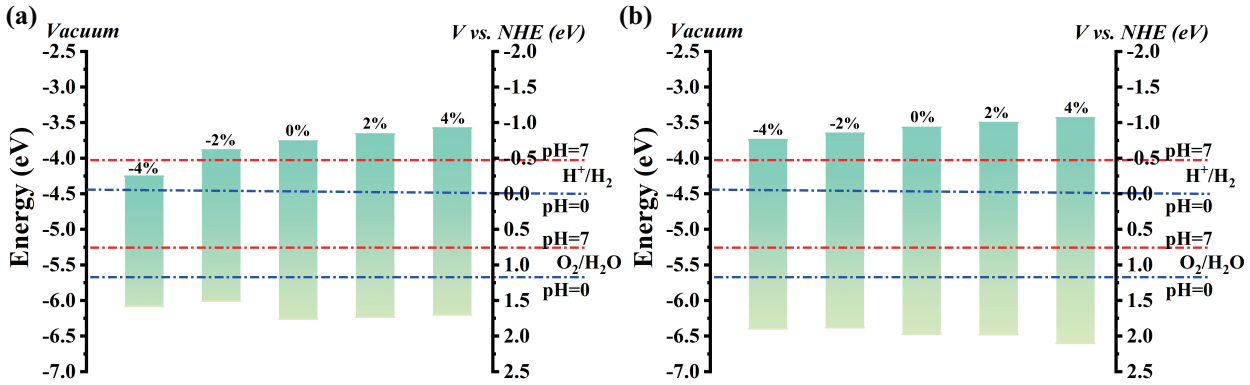

Figure S7. Redox potential of (a) p-$SiCC_4$/SnO and (b) p-$SiCC_4$/PbO heterojunctions for water splitting under biaxial strain.

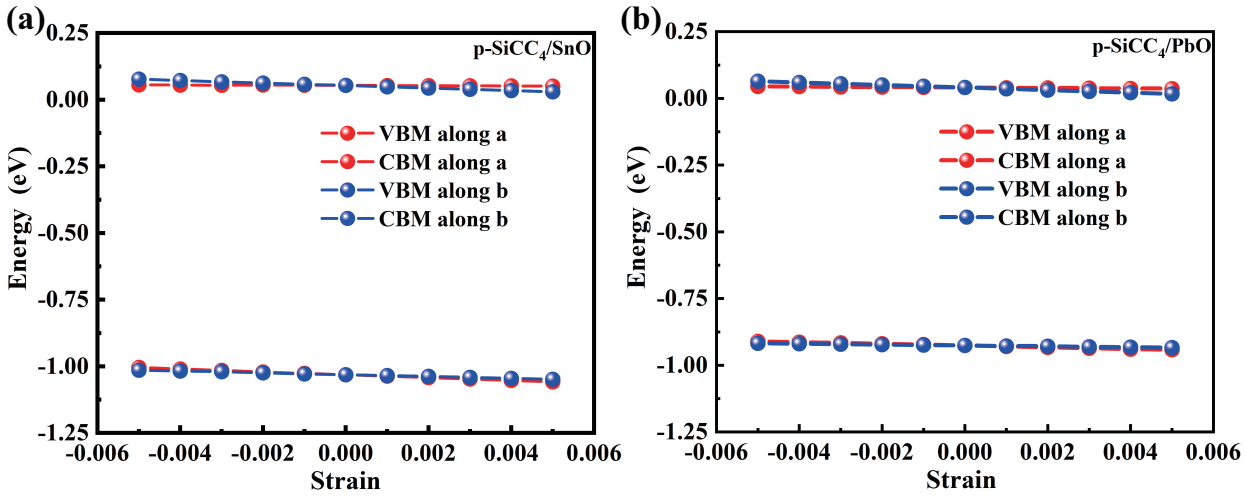

Figure S8. Band edge positions of CBM and VBM under uniaxial strain in (a) p-$SiCC_4$/SnO and (b) p-$SiCC_4$/PbO heterojunctions.

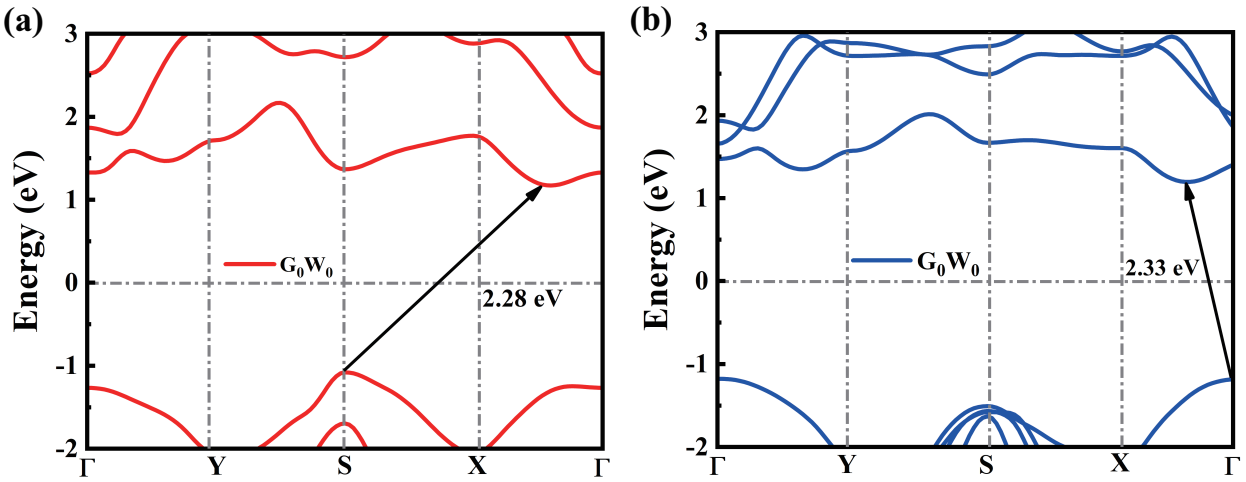

Figure S9. Quasiparticle electronic band structures of (a) p-$SiCC_4$/SnO and (b) p-$SiCC_4$/PbO heterojunctions calculated with the G_0W_0 functional.

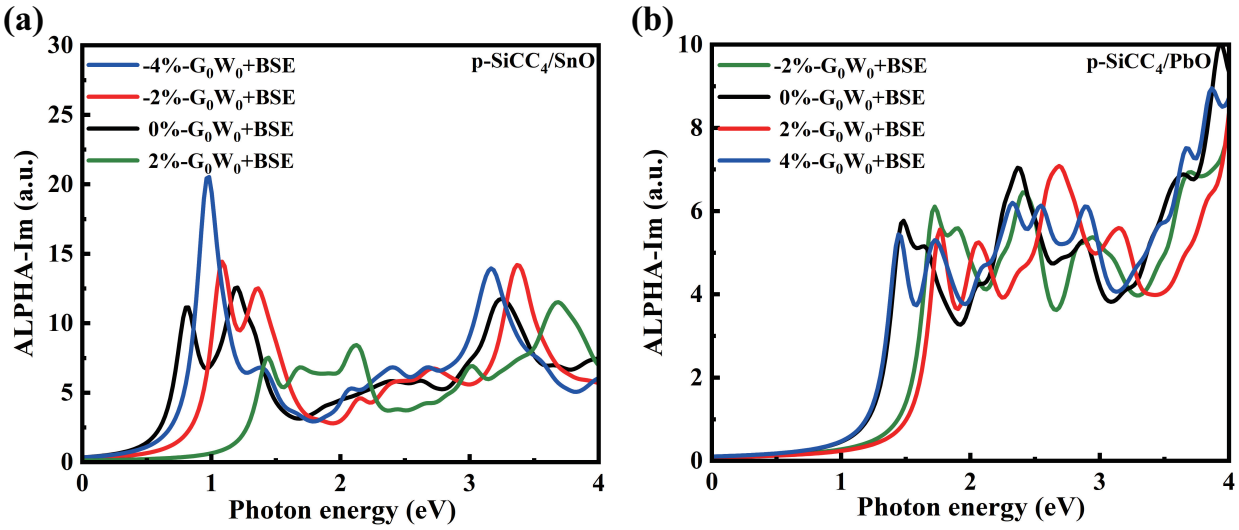

Figure S10. Tunable optical properties of (a) p-$SiCC_4$/SnO and (b) p-$SiCC_4$/PbO heterojunctions under biaxial strain.

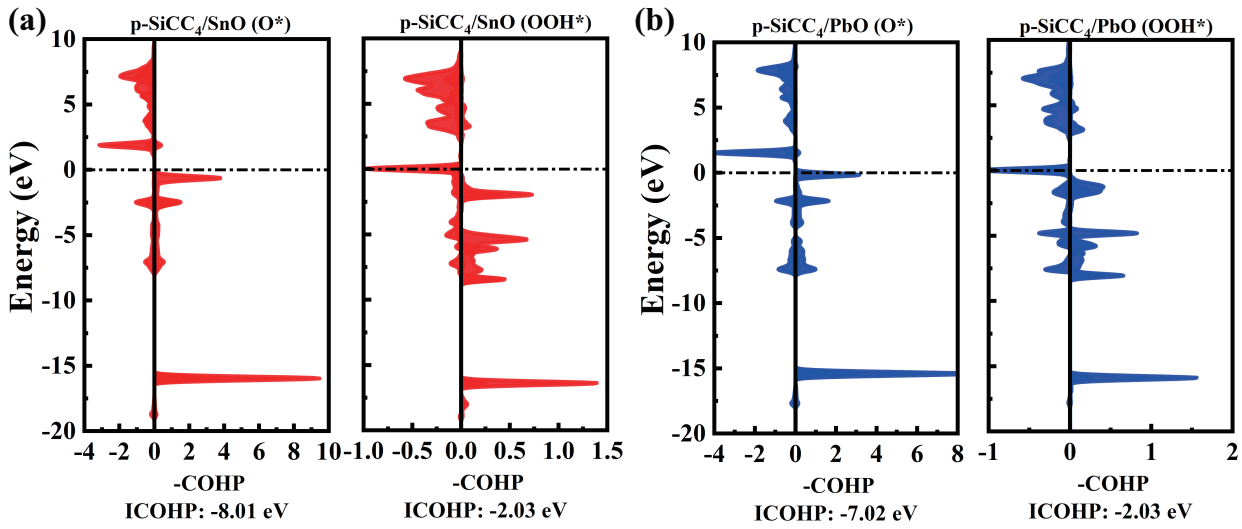

Figure S11. Projected COHP between the O atoms in the O* or OOH* states and the nearest neighboring Sn/Pb atoms in (a) p-$SiCC_4$/SnO, (b) p-$SiCC_4$/PbO heterojunctions.

Supplementary Notes

Note.1:

The charge density difference of p-$SiCC_4$/XO (X = Sn, Pb) heterojunctions is calculated by $\Delta\rho$=$\rho_{XO/SiCC_4}$-ρ_{XO}-ρ_{SiCC_4}, where $\rho_{XO/SiCC_4}$, ρ_{XO}, and ρ_{SiCC_4} represent the charge densities of the p-$SiCC_4$/XO (X = Sn, Pb) heterojunctions, XO (X = Sn, Pb), and p-$SiCC_4$ monolayer, respectively. The formula for the planar-averaged charge density difference is defined as $\Delta\rho(z) = \int \rho_{XO/SiCC_4}\mathrm{d}x\mathrm{d}y - \int \rho_{XO}\mathrm{d}x\mathrm{d}y - \int \rho_{SiCC_4}\mathrm{d}x\mathrm{d}y$, where $\int \rho_{XO/SiCC_4}\mathrm{d}x\mathrm{d}y$, $\int \rho_{XO}\mathrm{d}x\mathrm{d}y$, and $\int \rho_{SiCC_4}\mathrm{d}x\mathrm{d}y$ represent the vertical charge densities of p-$SiCC_4$/XO (X = Sn, Pb) heterojunctions, XO (X = Sn, Pb), and p-$SiCC_4$ perpendicular to the xy-plane, respectively.

Note.2:

We calculate carrier mobility of the p-$SiCC_4$/XO (X = Sn, Pb) heterojunctions based on the deformation potential (DP) theory[1], in Table. 2 and the corresponding equations are as follows

$$\mu^{2D} = \frac{2e\hbar^3 C^{2D}}{3k_{\mathrm{B}}T\left|m^*\right|^2 E_d^2} \tag{S1}$$

where e is the electron charge, $\hbar$ is the reduced Planck's constant, T is the temperature equal to 300 K throughout the paper. C^{2D} is the elastic modulus of a uniformly deformed crystal by strains and derived from $C^{2D} = [\partial^2 E/\partial^2(\Delta l/l_0)]/S_0$, in which E is the total energy, Δl is the change of lattice constant l_0 along the transport direction, and S_0 represents the area. The effective mass m^* of holes (m_h^*) and electrons (m_e^*) along the transport direction are obtained by fitting parabolic functions to the valence band maximum (VBM) and conduction band minimum (CBM), respectively, and given by $m^* = \hbar^2(\partial^2 E(k)/\partial k^2)^{-1}$ (k is wave-vector, and $E(k)$ denotes the energy) (either m_a^* or m_b^* along the $\boldsymbol{a}$ or $\boldsymbol{b}$ direction, respectively). E_d is the DP constant defined by $E_d^{e(h)} = \Delta E_{CBM(VBM)}/(\Delta l/l_0)$, where $\Delta E_{CBM(VBM)}$ is the energy shift of the band edge with respect to the vacuum level under a small dilation Δl of the lattice constant l_0.

Note.3:

The quasiparticle (QP) energies and optical properties are calculated within the framework of many-body perturbation theory and time-dependent density functional method, implemented by the Yambo and Quantum Espresso code[2]. The Hamiltonian considering

interacting electrons system can be expressed as the following Dyson equation[3, 4]

$$\left[-\frac{1}{2}\nabla^2 + V_{ion} + V_H + V_{xc}^{DFT} + (\Sigma(E^{QP})_{n\mathbf{k}} - V_{xc}^{DFT})\right]\psi_{n\mathbf{k}}^{QP} = E_{n\mathbf{k}}^{QP}\psi_{n\mathbf{k}}^{QP} \tag{S2}$$

where V_H is the Hartree term, V_{xc}^{DFT} is the DFT exchange-correlation potential, $E_{n\mathbf{k}}^{QP}$ and $\psi_{n\mathbf{k}}^{QP}$ represent QP eigen-energies and eigen-wavefunctions, respectively. And the self-energy operator Σ describes electron-electron interactions, which can be approximately obtained by $\Sigma = iG_0W_0$,

$$\Sigma\left(r, r'; \epsilon_n\right) = \frac{i}{2\pi}\int d\omega e^{i\omega 0^+} G_0\left(r, r'; \omega + \epsilon_n\right) W_0\left(r, r'; \omega\right) \tag{S3}$$

where the Green's function G_0 is constructed by Kohn-Sham (KS) orbitals, and W_0 is the frequency-dependent dynamically screened interaction defined as $W_0 = [1 - VP_0]^{-1}V$, where P_0 and V represent polarizability and bare Coulomb interaction, respectively.

Based on the GW approximation for the electronic self-energy Σ, adopting the random phase approximation (RPA) and the plasma pole approximation (PPA), the quasiparticle equation can be solved by taking the first order Taylor expansion of self-energy around the single-particle KS eigenenergy $\epsilon_{n\mathbf{k}}$,

$$E_{n\mathbf{k}}^{QP} = \epsilon_{n\mathbf{k}} + Z_{n\mathbf{k}}\langle\psi_{n\mathbf{k}}|\Sigma(\epsilon_{n\mathbf{k}}) - V_{xc}|\psi_{n\mathbf{k}}\rangle \tag{S4}$$

$$Z_{n\mathbf{k}} = \left[1 - \left.\frac{d\Sigma_{n\mathbf{k}}(\omega)}{d\omega}\right|_{\omega=\epsilon_{n\mathbf{k}}}\right]^{-1} \tag{S5}$$

where $E_{n\mathbf{k}}^{QP}$ denotes the quasiparticle energy of band n at wave vector $\mathbf{k}$, $\epsilon_{n\mathbf{k}}$ is the corresponding KS eigenvalue, $\psi_{n\mathbf{k}}$ is the associated KS wavefunction, $\Sigma(\omega)$ represents the frequency-dependent self-energy, V_{xc} is the exchange-correlation potential within DFT, and $Z_{n\mathbf{k}}$ is the quasiparticle renormalization factor, which accounts for the energy dependence of the self-energy and the weight of the quasiparticle excitation.

In PPA, the frequency dependence of the dielectric function $\varepsilon^{-1}_{\mathbf{G},\mathbf{G}'}(\mathbf{q},\omega)$ is modeled as a single-pole approximation:

$$\varepsilon^{-1}_{\mathbf{G},\mathbf{G}'}(\mathbf{q},\omega) = R_{\mathbf{G}\mathbf{G}'}(\mathbf{q})\left(\frac{1}{\omega - \omega_{\mathbf{G},\mathbf{G}'}(\mathbf{q}) + i\vartheta} - \frac{1}{\omega + \omega_{\mathbf{G},\mathbf{G}'}(\mathbf{q}) - i\vartheta}\right), \tag{S6}$$

where $\omega_{\mathbf{G},\mathbf{G}'}$ and $R_{\mathbf{G},\mathbf{G}'}(\mathbf{q})$ are the plasmon frequency and the real spectral function, respec-

tively. The inverse dynamical dielectric matrix, ε^{-1}, is derived below inside the random-phase approximation. To ensure convergence, the infnitesimally tiny positive value (ϑ) is added while performing a Fourier transformation from time to frequency space.

The quantitative description of the optical response of the interacting electron systems must be done by considering electron-hole interactions (exciton effects), which is achieved by solving the Bethe-Salpeter equation (BSE) [5, 6],

$$\left(E^{QP}_{c\mathbf{k}} - E^{QP}_{\nu\mathbf{k}}\right) A^{S}_{\nu c\mathbf{k}} + \sum_{\nu' c' \mathbf{k}'} \langle \nu c\mathbf{k}| \, K^{eh} \, |\nu' c' \mathbf{k}'\rangle \, A^{S}_{\nu' c' \mathbf{k}'} = \Omega_S A^{S}_{\nu c\mathbf{k}} \tag{S7}$$

where $E^{QP}_{c\mathbf{k},v\mathbf{k}}$ denotes the QP eigenvalues for electronic $|v\mathbf{k}\rangle$ and $|c\mathbf{k}\rangle$ states, $A^{S}_{vc\mathbf{k}}$ is the envelop function for the S^{th} exciton, the eigen state of which can be written as the summation over several electron-hole pairs, i.e., $|S\rangle = \sum_{\mathbf{k},v,c} A^{s}_{vck}|c\mathbf{k}\rangle \otimes |v\mathbf{k}\rangle$, and $|v\mathbf{k}\rangle/|c\mathbf{k}\rangle$ is the constituent electron/hole pair with identical momenta. Ω^S is the exciton eigen energy. The exciton wavefunction for the S^{th} exciton can be written by the summarization over the constituent electron-hole pair wavefunctions.

Then, the imaginary part of the dielectric function ϵ_2 can be calculated by[7],

$$\epsilon_2(\omega) = \frac{16\pi^2 e^2}{\omega^2} \sum_{S} |\mathbf{e} \cdot \langle 0|\mathbf{v}|S\rangle|^2 \delta(\omega - \Omega_S) \tag{S8}$$

where the matrix element $\langle 0|\mathbf{v}|S\rangle$ represents the optical transition dipole between the ground state $|0\rangle$ and the excited state $|S\rangle$ along the polarization direction $\mathbf{e}$, and the Dirac delta function ensures energy conservation for photon energy $\hbar\omega$.

The imaginary part of the electron self-energy $\Sigma_{n\mathbf{k}}$ represents the lifetime due to the quasi-particle effect, and the QP lifetime for $|n\mathbf{k}\rangle$ electron is calculated according to

$$\frac{1}{\tau_{n\mathbf{k}}} = \frac{2}{\hbar} \Im \Sigma_{n\mathbf{k}} \left(E^{QP}_{n\mathbf{k}}\right) \tag{S9}$$

Similar to equation, the lifetime limited by the electron-electron interactions for the S^{th} exciton can be written as[8],

$$\frac{1}{\tau^{S}_{ee}} = \sum_{\nu c\mathbf{k}} |A^{S}_{\nu c\mathbf{k}}|^2 \left(\frac{1}{\tau_{c\mathbf{k}}} + \frac{1}{\tau_{\nu\mathbf{k}}}\right) \tag{S10}$$

where $\tau_{\nu\mathbf{k}}/\tau_{c\mathbf{k}}$ are the lifetimes for the constituent valence hole/conduction electron pair, forming the S^{th} exciton.

Finally, the relaxation time for the S^{th} exciton induced by the direct recombination processes can be estimated as[9],

$$\gamma_S(\mathbf{Q}\to\mathbf{0}) = \tau_S(\mathbf{Q}\to\mathbf{0}) = \frac{8\pi e^2\Omega_S\mu_S^2}{S_0\hbar^2 c} \tag{S11}$$

where S_0 is the area of the unit cell, c is the speed of light, and μ_S^2 denotes the square modulus of the transition dipole moment for the exciton obtained from the BSE, given by

$$\mu_S^2 = \frac{\hbar^2}{m_e^2\Omega_S^2}\frac{|\langle G|p_\parallel|\Psi_S(0)\rangle|^2}{N_k} \tag{S12}$$

where m_e is the electron mass, and $\langle G|p_\parallel|\Psi_S(0)\rangle$ represents the momentum dipole matrix element in the exciton basis.

Note.4:

There are four steps to transform H_2O into O_2 molecule in oxidation half-reaction, which can be written as:

$$* + H_2O \to OH^* + H^+ + e^- \tag{S13}$$

$$OH^* \to O^* + H^+ + e^- \tag{S14}$$

$$O^* + H_2O \to OOH^* + H^+ + e^- \tag{S15}$$

$$OOH^* \to * + O_2 + H^+ + e^- \tag{S16}$$

For each electron reaction, species OH^*, O^*, and OOH^* and O_2 molecule in turn are the intermediates and final products. In the oxidation half-reaction, the adsorbed H_2O first releases a proton and an electron, making it become OH^*; Then, OH^* releases a proton and an electron, and becomes O^*; Next, O^* combines with another H_2O to release a proton and an electron, and O^* transforms into OOH^* species; Finally, OOH^* releases a proton and an electron again, resulting in a free O_2 molecule[10].

Meanwhile, hydrogen production half-reaction can be decomposed into two steps, the reaction equation can be written as[11]:

$$* + H^+ + e^- \to H^* \tag{S17}$$

$$H^* + H^+ + e^- \rightarrow * + H_2 \tag{S18}$$

We employed the method proposed by Nørskov et al[12], to calculate the free energy change (ΔG) of the photocatalytic reaction, as follows:

$$\Delta G = \Delta E + \Delta E_{\mathrm{ZPE}} - T\Delta S + \Delta G_{\mathrm{U}} + \Delta G_{\mathrm{pH}} \tag{S19}$$

Here, ΔE represents the adsorption energy, while ΔE_{ZPE} and ΔS correspond the differences in zero-point energy and entropy, respectively, between the adsorbed state and the gas phase. ΔG_{pH} ($\Delta G_{\mathrm{pH}} = k_{\mathrm{B}}T \times \ln 10 \times \mathrm{pH}$) denotes the free energy concentration contributed at various pH levels, where k_{B} is the Boltzmann constant and T denotes the absolute temperature. ΔG_{U} (ΔG_{U} = -eU) indicates the additional potential bias provided by electrons in the electrode, with e representing the electron charge.

For each oxidation and hydrogen production reaction, the free energy difference under the effect of pH and an extra potential bias can be written as[12]:

$$\Delta G_1 = G_{\mathrm{OH}^*} + \frac{1}{2}G_{\mathrm{H_2}} - G_* - G_{\mathrm{H_2O}} + \Delta G_{\mathrm{U}} - \Delta G_{\mathrm{pH}} \tag{S20}$$

$$\Delta G_2 = G_{\mathrm{O}^*} + \frac{1}{2}G_{\mathrm{H_2}} - G_{\mathrm{OH}^*} + \Delta G_{\mathrm{U}} - \Delta G_{\mathrm{pH}} \tag{S21}$$

$$\Delta G_3 = G_{\mathrm{OOH}^*} + \frac{1}{2}G_{\mathrm{H_2}} - G_{\mathrm{O}^*} - G_{\mathrm{H_2O}} + \Delta G_{\mathrm{U}} - \Delta G_{\mathrm{pH}} \tag{S22}$$

$$\Delta G_4 = G_* + \frac{1}{2}G_{\mathrm{H_2}} + G_{\mathrm{O_2}} - G_{\mathrm{OOH}^*} + \Delta G_{\mathrm{U}} - \Delta G_{\mathrm{pH}} \tag{S23}$$

$$\Delta G_5 = G_{\mathrm{H}^*} - \frac{1}{2}G_{\mathrm{H_2}} - G_* + \Delta G_{\mathrm{U}} + \Delta G_{\mathrm{pH}} \tag{S24}$$

$$\Delta G_6 = G_* + \frac{1}{2}G_{\mathrm{H_2}} - G_{\mathrm{H}^*} + \Delta G_{\mathrm{U}} + \Delta G_{\mathrm{pH}} \tag{S25}$$

In principle, achieving a complete water splitting requires photo-generated electrons and holes with sufficient energy to catalyze hydrogen evolution reaction (HER) and oxygen evolution reaction (OER). In the presence of solar radiation, the Photo-generated electronic potential (U_e) of HER is defined as the energy difference between the hydrogen reduction potential and the CBM. Conversely, the photo-generated hole potential (U_h) of OER is defined as the energy difference between the VBM and the hydrogen reduction potential.

The U_e and U_h at different pH levels can be determined by the following equation.

$$U_e = U_e(pH = 0) - pH \times 0.059 \tag{S26}$$

$$U_h = U_h(pH = 0) + pH \times 0.059 \tag{S27}$$

Supplementary Tables

Table S1. Calculated lattice constants (a, b), interlayer distances (d), bond lengths of Sn (Pb)-O (L_1), Si-C (L_2), C-C (L_3), and interface binding energies (E_b) of the p-$SiCC_4$/XO (X = Sn, Pb) heterojunctions.

Structure	a (Å)	b (Å)	L_1 (Å)	L_2 (Å)	L_3 (Å)	d (Å)	E_b (meV/Å^2)
p-$SiCC_4$/SnO							
H1	3.95	3.97	2.82	2.23	1.89	2.37	-29.626148
H2	3.95	3.97	2.82	2.23	1.89	2.37	-29.626143
H3	3.95	3.97	2.82	2.23	1.89	2.37	-29.626180
p-$SiCC_4$/PbO							
H1	4.00	4.02	3.04	2.23	1.89	2.54	-26.505930
H2	4.00	4.02	3.04	2.23	1.89	2.54	-26.505764
H3	4.00	4.02	3.04	2.23	1.89	2.54	-26.568600

Table S2. Effect of strain on exciton properties.

Material	Strain (%)	Indirect E_g	Direct E_g	E_1	exciton binding energy
p-$SiCC_4$/SnO	-4%	2.14	2.17	0.97	1.2
p-$SiCC_4$/SnO	-2%	2.23	2.38	1.08	1.3
p-$SiCC_4$/SnO	0%	2.28	2.42	0.8	1.62
p-$SiCC_4$/SnO	2%	2.22	2.32	1.43	0.89
p-$SiCC_4$/PbO	-2%	2.55	2.71	1.71	0.99
p-$SiCC_4$/PbO	0%	2.33	2.48	1.48	1
p-$SiCC_4$/PbO	2%	2.12	2.25	1.76	0.49
p-$SiCC_4$/PbO	4%	1.91	2.03	1.44	0.59

Table S3. Calculated the Gibbs free parameter values of the p-$SiCC_4$/SnO heterojunctions.

Species	ΔE (eV)	ΔE_{ZPE} (eV)	-TΔS (eV)	ΔG (eV)
H_2	-6.77	0.27	-0.41	-6.91
H_2O	-14.22	0.56	-0.67	-14.33
OH^*	-282.38	0.32	-0.16	-282.22
O^*	-278.06	0.05	-0.10	-278.10
OOH^*	-286.59	0.42	-0.23	-286.40
H^*	-275.92	0.28	-0.004	-275.64

Table S4. Calculated the Gibbs free parameter values of the p-$SiCC_4$/PbO heterojunctions.

Species	ΔE (eV)	ΔE_{ZPE} (eV)	-TΔS (eV)	ΔG (eV)
H_2	-6.77	0.27	-0.41	-6.91
H_2O	-14.22	0.56	-0.67	-14.33
OH^*	-278.05	0.31	-0.18	-277.92
O^*	-272.96	0.05	-0.12	-273.04
OOH^*	-282.45	0.41	-2.04	-284.08
H^*	-271.97	0.28	-0.004	-271.70

Table S5. The influence of strain on the electronic structure and photocatalytic efficiency of the p-$SiCC_4$/SnO heterostructure.

Strain (%)	$X(H_2)$	$X(O_2)$	E_g (eV)	ΔV	η_{abs} (%)	η_{cu} (%)	η_{STH} (%)	η'_{STH} (%)
-4	0.19	0.41	1.19	0.64	76.99	5.34	4.11	3.79
-2	0.55	0.34	1.83	0.53	44.65	34.86	15.56	14.87
0	0.65	0.57	2.00	0.45	36.62	49.00	17.94	16.87
2	0.78	0.56	2.17	0.40	29.41	43.67	12.84	12.32
4	0.86	0.53	2.27	0.36	25.61	40.43	10.35	10.05

Table S6. The influence of strain on the electronic structure and photocatalytic efficiency of the p-$SiCC_4$/PbO heterostructure.

Strain (%)	$X(H_2)$	$X(O_2)$	E_g (eV)	ΔV	η_{abs} (%)	η_{cu} (%)	η_{STH} (%)	η'_{STH} (%)
-4	0.70	0.93	2.13	0.73	31.05	47.1	14.62	13.45
-2	0.79	0.81	2.16	0.67	29.86	46.69	13.94	12.96
0	0.87	0.71	2.18	0.61	29.11	46.44	13.52	12.67
2	0.94	0.63	2.24	0.56	26.69	45.61	12.17	11.53
4	1.00	0.56	2.28	0.51	25.30	41.89	10.60	10.15

[1] J. Bardeen, W. Shockley, Deformation potentials and mobilities in non-polar crystals, Phys. Rev. 80 (1950) 72.

[2] D. Sangalli, A. Ferretti, H. Miranda, C. Attaccalite, I. Marri, E. Cannuccia, P. Melo, M. Mar-

sili, F. Paleari, A. Marrazzo, et al., Many-body perturbation theory calculations using the yambo code, J. Phys.: Condens. Matter 31 (2019) 325902.

[3] M. S. Hybertsen, S. G. Louie, Electron correlation in semiconductors and insulators: Band gaps and quasiparticle energies, Phys. Rev. B 34 (1986) 5390.

[4] L. Hedin, S. Lundqvist, Effects of electron-electron and electron-phonon interactions on the one-electron states of solids, in: Solid state physics, Vol. 23, Elsevier, 1970, pp. 1–181.

[5] M. Palummo, O. Pulci, R. Del Sole, A. Marini, P. Hahn, W. Schmidt, F. Bechstedt, The Bethe–Salpeter equation: a first-principles approach for calculating surface optical spectra, J. Phys.: Condens. Matter 16 (2004) S4313.

[6] M. Rohlfing, S. G. Louie, Electron-hole excitations and optical spectra from first principles, Phys. Rev. B 62 (2000) 4927.

[7] D. Y. Qiu, F. H. Da Jornada, S. G. Louie, Optical spectrum of MoS_2: many-body effects and diversity of exciton states, Phys. Rev. Lett. 111 (2013) 216805.

[8] K. F. Mak, F. H. Da Jornada, K. He, J. Deslippe, N. Petrone, J. Hone, J. Shan, S. G. Louie, T. F. Heinz, Tuning many-body interactions in graphene: The effects of doping on excitons and carrier lifetimes, Phys. Rev. Lett. 112 (2014) 207401.

[9] J. C. G. Maurizia Palummo, Marco Bernardi, Exciton radiative lifetimes in two-dimensional transition metal dichalcogenides, Nano Lett. 15 5 (2015) 2794–2800.

[10] L. Ju, M. Bie, X. Tang, J. Shang, L. Kou, Janus WSSe monolayer: an excellent photocatalyst for overall water splitting, ACS Appl. Mater. Interfaces 12 (2020) 29335–29343.

[11] S. Chen, L. W. Wang, Thermodynamic oxidation and reduction potentials of photocatalytic semiconductors in aqueous solution, Chem. Mater. 24 (2012) 3659–3666.

[12] J. K. Nørskov, J. Rossmeisl, A. Logadottir, L. Lindqvist, J. R. Kitchin, T. Bligaard, H. Jonsson, Origin of the overpotential for oxygen reduction at a fuel-cell cathode, J. Phys. Chem. B 108 (2004) 17886–17892.